Electrical Engineering
https://doi.org/10.1007/s00202-024-02557-8

ORIGINAL PAPER

Power system stabilizers tuning for probabilistic small-signal stability enhancement using particle swarm optimization and unscented transformation

Wesley Peres[1] · **Raphael P. B. Poubel**[2]

Received: 15 January 2024 / Accepted: 18 June 2024

Abstract
In modern power systems, uncertainties related to loads and renewable energy sources increase the need for reliable tools for steady-state and dynamic studies. These uncertainties are commonly modeled using probability density functions. In the context of the probabilistic small-signal stability analysis of power systems, the challenge lies in developing computationally efficient tools that accurately calculate the probability of ensuring security (minimum damping ratio greater than or equal to a desired value) and stability (negative spectral abscissa) requirements. This paper proposes an optimization approach for designing power system stabilizers to maximize the probability of meeting these security and stability requirements. The innovation of this approach is the integration of the unscented transformation (UT) with the particle swarm optimization (PSO). The UT is advantageous, as it requires a smaller number of samples to compute the mean and standard deviation of the output variables, especially compared to the Monte Carlo simulation (MCS), whereas PSO provides high-quality solutions. The New-England test system is employed in a case study to validate the proposed approach. This case study highlights the method's accuracy and computational efficiency advantages, showcasing its potential to address the challenges posed by increasing uncertainties in modern power systems.

Keywords PSS tuning · Small-signal stability enhancement · Particle swarm optimization · Unscented transformation · Probabilistic analysis

Abbreviations

2PEM	Two-point estimate method
BA	Bat algorithm
CCA	Cooperative coevolutionary algorithm
CS	Cuckoo search
D-SSSA	Deterministic small-signal stability assessment
DBA	Directional bat algorithm
DE	Differential evolution
ESS	Energy storage system
FFOA	Fruit fly optimization algorithm
FO	Firefly optimization
GA	Genetic algorithm
VSC-HVDC	Voltage source converters based high voltage direct current systems
LFO	Low-frequency oscillations
LHS	Latin hypercube sampling
MCS	Monte Carlo simulation
MICA	Modified imperialist competitive algorithm
PID-PSS	Proportional-integral-derivative PSS
P-SSSA	Probabilistic small-signal stability assessment
PDF	Probability density functions
POD	Power oscillation damper
PSO	Particle swarm optimization
PSS	Power system stabilizer
PV	Photovoltaic systems
STATCOM	Static synchronous compensators

Wesley Peres and Raphael P. B. Poubel have contributed equally to this work.

✉ Wesley Peres
wesley.peres@ufsj.edu.br

Raphael P. B. Poubel
poubel@cefetmg.br

[1] Department of Electrical Engineering, Federal University of São João del-Rei - UFSJ, São João del-Rei, Brazil

[2] Department of Electrical Engineering, Federal Center of Technological Education of Minas Gerais - CEFET-MG, Belo Horizonte, Brazil

Published online: 02 July 2024

SSSA	Small-signal stability assessment
UT	Unscented transformation
WG	Wind generator.

1 Introduction

Low-frequency oscillations (LFO) in power systems are mainly caused by imbalances in mechanical and electrical torques at synchronous generators following minor disturbances, such as variations in load or changes in controller reference values [1]. These oscillations have been a significant topic of study in the power systems literature since the 1970 s [2–5]. The predominant strategy for damping these oscillations involves the implementation of power oscillation dampers (POD). Among various PODs, the power system stabilizer (PSS) is the most recognized, installed at synchronous generators. The PSS modulates the field voltage during transient events, thereby helping dampen the LFO [1, 6, 7].

Small-signal stability assessment (SSSA) is essential for studying LFO and PSS tuning. This assessment involves linearizing the power system model at a specific operating condition. Subsequently, the angular stability of the system is evaluated through modal analysis, which is essentially based on the calculation of eigenvalues, as detailed in [7].

In contemporary power systems, uncertainties in loads and renewable energy generation are critical in the planning and operational stages. Traditional deterministic small-signal stability assessment (D-SSSA) does not account for these uncertainties, which can lead to imprecise results, as highlighted in [8, 9]. Consequently, probabilistic approaches to small-signal stability assessment (probabilistic SSSA, P-SSSA) have become increasingly relevant. P-SSSA specifically addresses the challenge of computing the mean and standard deviation of the output variables (minimum damping ratio and spectral abscissa) from the mean and standard deviation of the input variables (loads and powers generated from renewable sources). Recently, [10] emphasized the importance of considering uncertainties in scenarios with a high penetration of renewable energy sources. This consideration is crucial regardless of the technology employed for power oscillation damping [10].

As described in [8] [11], approaches for performing probabilistic analyzes in power systems can be classified into three main categories: (*i*) analytical, (*ii*) numerical and sampling-based, and (*iii*) approximate methods.

Numerical and sampling methods, including Monte Carlo Simulation (MCS), Latin Hypercube Sampling, and Quasi-MCS, play a crucial role in probabilistic analyses in power systems. MCS, in particular, relies on generating many samples for random input variables (like loads and generations), applying the nonlinear model to each sample to obtain output variables, and then calculating statistical variables (mean and standard deviation) for each output. Despite its accuracy, MCS is known for its high computational demand. For example, in [12] a quasi-MCS technique is proposed for P-SSSA, considering uncertainties related to electric vehicles and wind generation. Similarly, [13] introduces an approach to the probabilistic design of conventional PSS in synchronous generators, focusing on maximizing the probability of meeting the system security requirements under uncertainties in wind generation. This method utilizes a combination of Genetic Algorithm and MCS. A Latin hypercube sampling-based approach has been proposed in [14] for the probabilistic design of conventional PSS at synchronous generators and POD at wind generators. This method aims to maximize the number of stable scenarios and employs differential evolution for problem-solving. A cooperative coevolutionary algorithm and the MCS for the probabilistic design of conventional PSS is proposed in [15]. This approach considers uncertainties in wind powers and loads. A framework based on Monte Carlo simulation for stochastic eigenvalue analysis of electric power systems is proposed in [16]. This framework, which addresses systems with high penetration of inertialess renewable generation, focuses on the influential factors affecting eigenvalue movement due to reduced inertia. In [17], Monte Carlo simulation is used to calculate the probability of occurrence of unstable scenarios resulting from network failures. In [18], the MCS is used to propose a framework for defining multi-stability operational boundaries of power systems. This framework takes into account varying penetration levels of power electronic interfaced generation and the uncertainty in system loading. Finally, [19] employs MCS to evaluate probabilistic stability, considering controllers designed by classical methods.

Analytical approaches such as the cumulant method have been proposed to minimize the computational cost of numerical-based methods. These methods rely on linearizing equations and provide results with a lower computational burden. However, significant fluctuations in input random variables can lead to substantial linearization errors. In [20], the differential evolution and an analytical method based on Taylor series are combined for the probabilistic design of conventional PSS considering load uncertainties. Conventional PSS for synchronous generators and power oscillation damping (POD) at static voltage compensators are designed in [9], taking into account uncertainties in wind power using the cumulant method and the fruit fly optimization algorithm. The paper [21] employs four bio-inspired optimization algorithms (bat algorithm, cuckoo search, firefly algorithm, and particle swarm optimization) along with the cumulant method for probabilistic tuning of conventional PSS and POD in wind generators and solar panels. The probabilistic design of conventional PSS is executed using the cumulant method and the directional bat algorithm in [22], considering the uncertainties of power load and wind generation. In

[23], the cumulant method and the firefly optimization algorithm are utilized to design conventional PSS for synchronous generators and POD in energy storage systems. In [24], a surrogate method using deep learning, the bat algorithm-based optimization, and the cumulant method are integrated for a probabilistic design of POD controllers of wind and photovoltaic generators. In [25], the probabilistic small-signal stability in systems with uncertain wind power is evaluated by series expansion and maximum entropy theory, providing excellent accuracy and sufficient efficiency.

A balance between accuracy and efficiency in system analysis can be achieved by employing approximate methods like the unscented transformation (UT) [26] and two-point estimate method (2PEM) [27]. These methods determine a reduced number of samples in a deterministic way. The 2PEM is used in [28] to assess the power system small-signal stability analysis (P-SSSA). In [29], the impact of wind generation uncertainty in systems equipped with conventional PSS—not subject to tuning—is evaluated using the 2PEM. [30] discusses a probabilistic design of conventional PSS for synchronous generators and POD for wind generators and static synchronous compensators (STATCOM), utilizing the modified imperialist competitive algorithm and the 2PEM. In [31], the gradient optimization method and the 2PEM are utilized to optimize the virtual inertia and pitch angle parameters of wind turbines.

Finally, in [32], it is proposed an optimal procedure to design a robust PID-PSS using interval arithmetic for the single-machine infinite bus system. Interval methods, while helpful in ensuring safety under uncertainty, have notable disadvantages compared to probabilistic methods. They do not provide probability distributions within established ranges, leading to overly conservative solutions that may be less efficient and more costly. In addition, interval methods suffer from high computational complexity in large-scale problems, as they consider all possible values within limits.

Table 1 summarizes the publications mentioned above. This review highlights that the area of probabilistic design for power system stabilizers and power oscillation damping controllers, particularly employing bio-inspired optimization techniques together with the unscented transformation, remains unexplored. The UT is an approximate technique based on a reduced set of samples called sigma points, which are deterministically calculated.

1.1 Main contributions

This paper introduces a novel optimization approach for enhancing the probabilistic design of conventional power system stabilizers (PSS) in transmission systems. Leveraging particle swarm optimization (PSO) in tandem with unscented transformation (UT), the method aims to maximize the probabilities of meeting predefined thresholds for both the minimum damping ratio (small-signal security) and the spectral abscissa (small-signal stability). A key innovation lies in the utilization of UT to evaluate each individual of the PSO within a probabilistic small-signal stability assessment (P-SSSA), which constitutes the primary contribution of this research.

To capture the uncertainties inherent in loads and wind power generation, the model uses a normal distribution. The efficacy of the approach is demonstrated through a comprehensive case study using the New-England test system [33]. Furthermore, validation is conducted via nonlinear time-domain simulations.

Of particular significance, the proposed probabilistic tuning method exhibits superior performance compared to deterministic approaches, especially when subjected to scenarios unforeseen during the design phase. This underscores the robustness and practical applicability of the methodology in real-world transmission systems.

2 Background: probabilistic small-signal stability assessment

2.1 Deterministic small-signal stability

The small-signal stability analysis of transmission systems employs linearized models considering specific operational conditions. These conditions are provided by the power flow solution corresponding to a given load and generation profiles. The linearized models are represented through state-space formulations, both in open-loop and closed-loop configurations.

Figure 1 illustrates the static excitation system of a synchronous generator. This system's primary function is to ensure that the terminal voltage, denoted as ΔV_T, remains consistent with the reference value, ΔV_{REF}, achieved by controlling the field voltage ΔE_{FD}. In this static excitation system model, the parameters K_A and T_A correspond to the gain and the time constant, respectively [7]. Additionally, in Fig. 1, the transfer function of the power system stabilizer, $PSS(s)$, is distinctly highlighted in red. This controller interacts with the excitation system during transient events, introducing a supplementary signal, ΔV_{PSS}, to ensure the power system's stability [2]. Notably, in this configuration, the stabilizer's input signal is derived from the synchronous generator terminal velocity $\Delta\omega$, though alternative input types could also be adopted [7].

From Fig. 1, two distinct operational modes can be identified: (*i*) open-loop operation (without the PSS) and (*ii*) closed-loop operation (incorporating the PSS). The state-space representation corresponding to the open-loop operation is delineated in (1). For completeness, the differential equations associated with the generator and automatic volt-

Table 1 Publications on recent P-SSSA

Year	Probabilistic method	Optimal tuning?	Controller	Reference
2007	2PEM	Only assessment	–	[28]
2008	Taylor series	DE	PSS-SG	[20]
2012	2PEM	Only assessment	PSS-SG	[29]
2013	Quasi-MCS	Only assessment	PSS-SG	[12]
2014	MCS	GA	PSS-SG	[13]
2015	Cumulant	FFOA	PSS-SG, POD-SVC	[9]
2016	LHS	DE	PSS-SG, POD-WG	[14]
2019	Cumulant	BA, CS, FO, PSO	PSS-SG, POD-WG	[21]
2019	2PEM	MICA	PSS-SG, POD-WG POD-STATCOM	[30]
2020	Cumulant	DBA	PSS-SG	[22]
2020	Cumulant	FO	PSS-SG, POD-ESS	[23]
2020	MCS	CCA	PSS-SG	[15]
2020	MCS	Only assessment	PSS-SG	[16]
2020	Interval arithmetic	Gradient method	PID-PSS-SG	[32]
2021	Cumulant	BA	POD-WG, POD-PV	[24]
2021	MCS	Only assessment	PSS-SG	[19]
2021	MCS	Only assessment	PSS-SG	[17]
2022	2PEM	Gradient method	Virtual inertia and WG parameters	[31]
2022	MCS	Only assessment	VSC-HVDC	[18]
2024	Series expansion and maximum entropy theory	Only assessment	PSS-SG	[25]
2024	UT	PSO	PSS-SG	Proposed

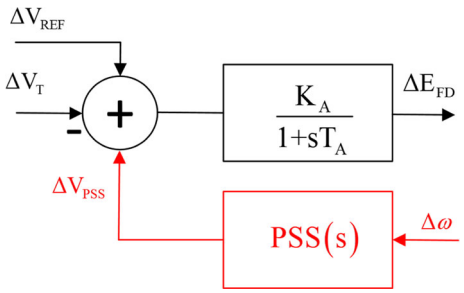

Fig. 1 Static excitation system

age regulator models are presented in Appendix A.

$$\begin{aligned} \Delta\dot{x} &= A_O \Delta x + B_O \Delta u \\ \Delta y &= C_O \Delta x \end{aligned} \tag{1}$$

where

- A_O, B_O, and C_O are the state-space, input, and output matrices, respectively;
- Δx represents the vector of states, encompassing angular speeds, internal angles, internal voltages, and field voltages. Similarly, Δu denotes the vector containing input values, specifically ΔV_{REF}, while Δy signifies the vector associated with output variables, in this case, $\Delta\omega$.

The state-space model for closed-loop operation, denoted by the subscript C in (2), is derived from (1) using a feedback procedure that takes into account the transfer function of the PSS, as defined in (3) [7].

$$\begin{aligned} \Delta\dot{x} &= A_C \Delta x + B_C \Delta u \\ \Delta y &= C_C \Delta x \end{aligned} \tag{2}$$

$$PSS_p(s) = K_p \frac{sT_w}{1+sT_w} \left(\frac{1+s\frac{\sqrt{\alpha_p}}{\omega_p}}{1+s\frac{1}{\omega_p\sqrt{\alpha_p}}} \right)^{nb} \tag{3}$$

where (for the p^{th} generator)

- $PSS_p(s)$ represents the transfer function of the PSS;
- T_w denotes the time constant of the *washout* filter, ensuring that the PSS operates exclusively during transients;
- K_p is the gain associated with the PSS;
- α_p and ω_p specify the parameters for the lead-lag stage of the PSS, which serves as the phase compensation stage;
- nb indicates the total number of lead-lag stages.

Each PSS comprises five parameters that require tuning: $K_p, \alpha_p, \omega_p, T_w$, and nb. Typically, T_w and nb are predefined, leaving only the gain and the two lead-lag parameters to be

fine-tuned. Consequently, for a system with ng generators equipped with PSS, a total of $3 \times ng$ parameters require design adjustments [34–36].

Once the state-space representation is obtained, it is possible to evaluate the small-signal stability through the modal analysis. It is done by calculating the m eigenvalues for a state-space matrix (order $m \times m$). Equation (4) brings the i^{th} eigenvalue (with real σ_i and imaginary ω_i components), whose damping ratio ξ_i is calculated according to (5). The system is stable when all σ_i are negative and ξ_i are positive [7].

$$\lambda_i = \sigma_i \pm j\omega_i \tag{4}$$

$$\xi_i = \frac{-\sigma_i}{\sqrt{\sigma_i^2 + \omega_i^2}} \tag{5}$$

In the context of deterministic small-signal analysis, establishing the minimum damping ratio $\xi_{\min}$ and the spectral abscissa $\sigma_{\max}$ is essential. It is made according to (6). In power system operation, we say that the power system is secure when its minimum damping ratio $\xi_{\min}$ is greater than or equal to a security level (10%, for instance) [37].

$$\begin{aligned} \sigma_{\max} &= \max(1, \ldots, \sigma_i, \ldots, \sigma_m) \\ \xi_{\min} &= \min(1, \ldots, \xi_i, \ldots, \xi_m) \end{aligned} \tag{6}$$

In the context of power system analysis, we refer to deterministic small-signal analysis when all loads and generation from renewable sources are precisely known. However, a more comprehensive probabilistic analysis becomes essential when uncertainties are incorporated. This will be the focus of the subsequent subsection.

2.2 Probabilistic model of loads and renewable energy

In the present study, we perform a probabilistic analysis, accounting for uncertainties both in active and reactive power loads as well as in the generation from renewable sources, specifically wind generation. These uncertainties are modeled employing the Normal Distribution as depicted in (7) [15, 22, 23, 38].

$$f(P_{dk}) = \frac{1}{\sigma_{P_{dk}}\sqrt{2\pi}} e^{-\frac{\left(P_{dk} - \mu_{P_{dk}}\right)^2}{2\sigma^2_{P_{dk}}}}$$

$$f(Q_{dk}) = \frac{1}{\sigma_{Q_{dk}}\sqrt{2\pi}} e^{-\frac{\left(Q_{dk} - \mu_{Q_{dk}}\right)^2}{2\sigma^2_{Q_{dk}}}}$$

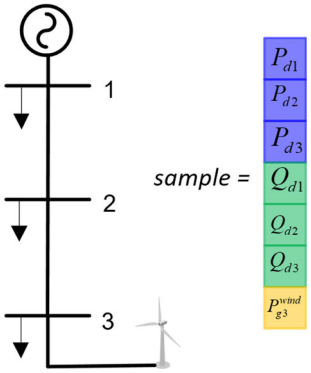

Fig. 2 Illustrative example of a sample

$$f\left(P_{gk}^{\text{wind}}\right) = \frac{1}{\sigma_{P_{gk}^{\text{wind}}}\sqrt{2\pi}} e^{-\frac{\left(P_{gk}^{\text{wind}} - \mu_{P_{gk}^{\text{wind}}}\right)^2}{2\sigma^2_{P_{gk}^{\text{wind}}}}} \tag{7}$$

where

- $\mu_{P_{dk}}$, $\mu_{Q_{dk}}$, and $\mu_{P_{gk}^{\text{wind}}}$ represent the mean values of loads and wind generation at a node k;
- $\sigma_{P_{dk}}$, $\sigma_{Q_{dk}}$, and $\sigma_{P_{gk}^{\text{wind}}}$ represent the standard deviations of loads and wind generation at a node k.

2.3 Procedure for probabilistic small-signal assessment using the Monte Carlo simulation

The probabilistic evaluation of the small-signal stability consists of calculating the mean ($\mu_{\sigma_{\max}}$ and $\mu_{\xi_{\min}}$) and standard deviation ($\sigma_{\sigma_{\max}}$ and $\sigma_{\xi_{\min}}$) values of the spectral abscissa and the minimum damping ratio, taking into account the uncertainties on loads and generation of renewable sources (see Sect. 2.2).

The Monte Carlo simulation is the predominant method for probabilistic analysis, utilizing a suite of random samples in its numerical approach. Figure 2 provides an illustrative example, showcasing a sample vector for a system comprising three buses and one wind generator.

Figure 3 outlines the procedure to evaluate probabilistic small-signal stability using the Monte Carlo simulation. In **Step 1**, the necessary number of samples, power system data (including nodes and branches), and stabilizer parameters are imported. Moving to **Step 2**, a sample, as exemplified in Fig. 2, is generated following Eq. (7). For **Step 3**, the state-space model in open-loop operation is established by solving the power flow and then linearizing the nonlinear system [7, 36]. In **Step 4**, a feedback procedure calculates the closed-loop state-space model, incorporating all the power system stabilizers. **Step 5** then computes the minimum damping ratio and the spectral abscissa based on (6). After storing the values

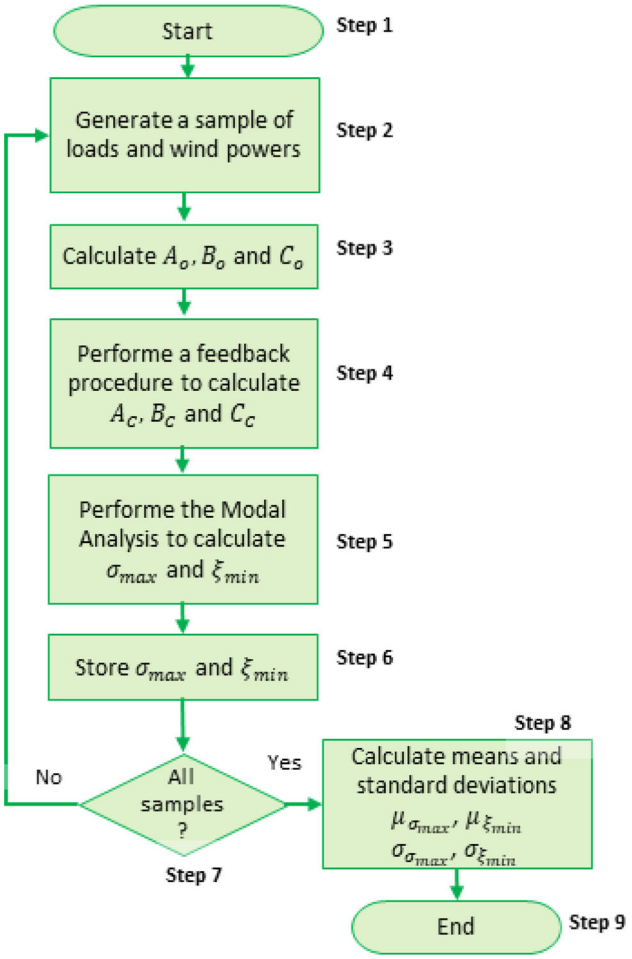

Fig. 3 Flowchart—Monte Carlo Simulation

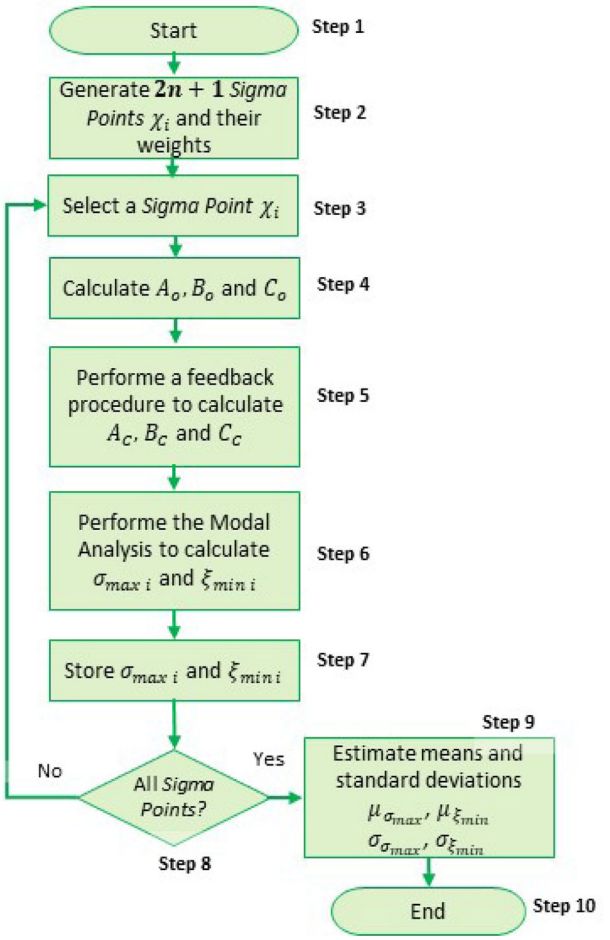

Fig. 4 Flowchart—unscented transform based small-signal analysis

of $\sigma_{\max}$ and $\xi_{\min}$ in **Step 6**, **Step 7** verifies if the desired number of samples has been achieved. If achieved, **Step 8** calculates the mean and standard deviations, concluding the process in **Step 9**. If not, the procedure returns to **Step 2** to generate another sample. For the sake of completeness, an illustrative example is presented in Appendix D.

2.4 Procedure for probabilistic small-signal assessment using the unscented transformation

The unscented transformation method employs a reduced set of samples deterministically calculated so that the computational burden is significantly lower compared with the Monte Carlo simulation. Each sample is referred to as a sigma point $\boldsymbol{\chi_i}$ with the same structure shown in Fig. 2. Figure 4 brings the steps required to assess the small-signal stability through the unscented transformation. **Step 1** and **steps 4 to 7** are similar to **step 1** and **steps 3 to 6** of Fig. 3, respectively.

Firstly, the vector of means z_m and the matrix with variances P_z are defined according to Eq. (8) in **Step 1**. Considering nb load nodes and $nren$ nodes with wind generators, the dimensions of z_m and P_z are $((2nb + nren) \times 1)$ and $((2nb + nren) \times (2nb + nren))$, respectively.

$$z_m = \begin{bmatrix} \mu_{P_{dk}} \\ \mu_{Q_{dk}} \\ \mu_{P_{gi}^{\text{wind}}} \end{bmatrix}$$
$$P_z = \begin{bmatrix} \sigma^2_{P_{dk}} & 0 & 0 \\ 0 & \sigma^2_{Q_{dk}} & 0 \\ 0 & 0 & \sigma^2_{P_{gi}^{\text{wind}}} \end{bmatrix} \tag{8}$$

where $k = 1, \cdots, nb$ and $i = 1, \cdots, nren$.

Being n uncertain variables (in this paper $n = 2nb + nren$), in **Step 2** $2n + 1$, sigma points are calculated. Each sigma point χ_i is a column vector representing a sample whose structure follows the one shown in Fig. 2. Different from the Monte Carlo simulation, sigmas points are deterministically calculated according to Eqs. (9)–(11).

$$\chi_1 = z_m \tag{9}$$
$$\chi_{i+1} = z_m + u_i, \quad i = 1, \ldots, n \tag{10}$$

$$\chi_{i+1} = z_m - u_i, \quad i = 1, \ldots, n \tag{11}$$

where u_i is a row vector of the matrix U, computed using the Cholesky decomposition, as presented in Eq. (12) [26].

$$U^T U = (n + \kappa) P_z \tag{12}$$

In (12), κ is a parameter empirically tuned so that the results (means and variances of output variables) are close to those provided by the Monte Carlo simulation [39, 40]. In this paper, $\kappa = 0$ is considered.

For each sigma point, it is performed a deterministic small-signal analysis (**Steps 4 to 7** in Fig. 4) to obtain the minimum damping ratio and the spectral abscissa based on (6): $\sigma_{\max i}$ and $\xi_{\min i}$ (here, i denotes the i^{th} sigma point).

Once all sigma points are evaluated, the means ($\mu_{\sigma_{\max}}$ and $\mu_{\xi_{\min}}$) and standard deviations ($\sigma_{\sigma_{\max}}$ and $\sigma_{\xi_{\min}}$) of output variables are estimated in **Step 9** by (13)-(14). For this purpose, weight factors W_i are required.

$$\begin{aligned} \mu_{\sigma_{\max}} &= \sum_{i=1}^{2n+1} W_i \cdot \sigma_{\max i} \\ \mu_{\xi_{\min}} &= \sum_{i=1}^{2n+1} W_i \cdot \xi_{\min i} \end{aligned} \tag{13}$$

$$\begin{aligned} \sigma_{\sigma_{\max}} &= \sqrt{\sum_{i=1}^{2n+1} W_i \cdot \left(\mu_{\sigma_{\max}} - \sigma_{\max i}\right)^2} \\ \sigma_{\xi_{\min}} &= \sqrt{\sum_{i=1}^{2n+1} W_i \cdot \left(\mu_{\xi_{\min}} - \xi_{\min i}\right)^2} \end{aligned} \tag{14}$$

The weight factors W_i are obtained by (15)-(17). It is important to say that the sum of all weights must be equal to unity (see (18)).

$$W_1 = \frac{\kappa}{n + \kappa} \tag{15}$$

$$W_{i+1} = (2(n + \kappa))^{-1}, i = 1, \ldots, n \tag{16}$$

$$W_{i+n+1} = (2(n + \kappa))^{-1}, i = 1, \ldots, n \tag{17}$$

$$\sum_{i=1}^{2n+1} W_i = 1 \tag{18}$$

2.5 Confidence levels

According to [37], a system is considered to be secure from the angular small-signal point of view if its minimum damping ratio $\xi_{\min}$ is greater than or equal to a desired security margin ξ_d. In the context of probabilistic small signal, it is essential to define the security using probabilities as given in (19):

$$\begin{aligned} P_r\{\xi_{\min} \geq \xi_d\} &\geq \gamma_{\xi_{\min}} \\ P_r\{\sigma_{\max} \leq 0\} &\geq \gamma_{\sigma_{\max}} \end{aligned} \tag{19}$$

where $\gamma_{\xi_{\min}}$ and $\gamma_{\sigma_{\max}}$ are the confidence levels. It is important to say that probabilities are calculated by using the values of means and standard deviations in (13)- (14).

3 Proposed approach for PSS tuning

3.1 Optimization approach

The main contribution of this paper is an optimization approach for the probabilistic design of power system stabilizers. The optimization uses the particle swarm optimization [41], and the unscented transformation performs the probabilistic analysis.

The mathematical formulation of the proposed approach is presented in (20)-(25). The objective function in (20) aims to maximize the probabilities of satisfying the minimum damping ratio requirement ($\xi_{\min} \geq \xi_d$) and the stability (given by the spectral abscissa $\sigma_{\max}$). Equation (21) ensures that the mean value of the minimum damping ratio $\mu_{\xi_{\min}}$ is greater than or equal to the security margin (ξ_d). Additionally, (22) ensures that the mean value of the spectral abscissa $\mu_{\sigma_{\max}}$ is negative (condition to stability). Finally, the parameters to be tuned (K_p, α_p, and ω_p) must be into the limits, as constrained in (23)-(25).

$$\max f(x) = P_r\{\xi_{\min} \geq \xi_d\} + P_r\{\sigma_{\max} < 0\} \tag{20}$$

$$\text{s.t.} \quad \mu_{\xi_{\min}} \geq \xi_d \tag{21}$$

$$\mu_{\sigma_{\max}} < 0 \tag{22}$$

$$K_p^{\min} \leq K_p \leq K_p^{\max} \tag{23}$$

$$\alpha_p^{\min} \leq \alpha_p \leq \alpha_p^{\max} \tag{24}$$

$$\omega_p^{\min} \leq \omega_p \leq \omega_p^{\max} \tag{25}$$

where $p = 1, \ldots, npss$, being $npss$ the number of stabilizers to be tuned. Each PSS has the transfer function defined in (3).

3.2 Fitness function calculation

Solving the optimization problem in (20)-(25) through an analytical approach is hard, and this paper uses particle swarm optimization for this task. It is a population-based method in which each individual represents a solution for the problem. In this section, the process to calculate the fitness function of each individual is presented.

In this paper, an individual ind_i is a vector with the values of gains and parameters of the compensation stage (a possible solution) as defined in (26). The quality of the tuning provided by this individual is measured by its fitness function fit_i, calculated according to (27).

The fitness function fit_i in (27) is composed of three parts: F_1, F_2, and F_3. The first component (F_1) is defined in (28) and deals with the objective function in (20). The second and third components (F_2 and F_3 defined in (29)-(30)) are necessary to deal with the constraints (21) -(22). They are applied penalizations in case of violations ($\xi_{\min} < \xi_d$ or $\sigma_{\max} > 0$). Each component has its weight β, empirically defined.

$$ind_i = \left[K_1 \ldots K_{npss}\ \alpha_1 \ldots \alpha_{npss}\ \omega_1 \ldots \omega_{npss} \right] \tag{26}$$

$$fit_i = \beta_1 \cdot F_1 - \beta_2 \cdot F_2 - \beta_3 \cdot F_3 \tag{27}$$

where $\beta_1 = 1$ and $\beta_2 = \beta_3 = 10^4$.

$$F_1 = P_r\left\{\xi_{\min} \geq \xi_d\right\} + P_r\left\{\sigma_{\max} < 0\right\} \tag{28}$$

$$F_2 = \begin{cases} \mid penal_1 \mid & \text{if } \mu_{\xi_{\min}} < \xi_d \\ 0 & \text{otherwise} \end{cases} \tag{29}$$

where $penal_1 = \xi_d - \mu_{\xi_{\min}}$.

$$F_3 = \begin{cases} \mid penal_2 \mid & \text{if } \mu_{\sigma_{\max}} \geq 0 \\ 0 & \text{otherwise} \end{cases} \tag{30}$$

where $penal_2 = \mu_{\sigma_{\max}}$.

It is important to say that constraints (23)-(25) are directly handled by the PSO method for constrained optimization.

Finally, Fig. 5 brings an illustrative example regarding the Fitness Function fit_i evaluation for a given individual ind_i. The first step is to perform a probabilistic small-signal stability analysis through the unscented transformation to calculate the means and standard deviations of the minimum damping ratio ($\mu_{\xi_{\min}}$ and $\sigma_{\xi_{\min}}$) and the spectral abscissa ($\mu_{\sigma_{\max}}$ and $\sigma_{\sigma_{\max}}$), as discussed in Sect. 2.4 and Fig. 4. These values are used to calculate the probabilities in (20) and (28) [42]. Finally, the fitness function fit_i is calculated as defined in (27)-(30).

3.3 Optimization methodology flowchart

As discussed in Sect. 3.2, the proposed approach in (20)-(25) is solved by the particle swarm optimization method. In addition, the calculation of the fitness function is illustrated in Fig. 5. Figure 6 illustrates the integration of the PSO method and the unscented transformation for the probabilistic analysis of small-signal stability.

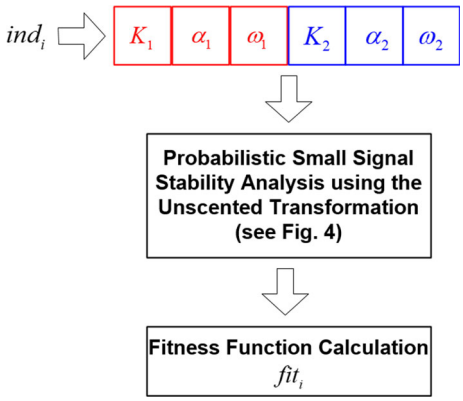

Fig. 5 Fitness function evaluation

The optimization method unfolds in a systematic manner. It commences in **Step 1** with the definition of variable limits and the PSO and UT parameters. **Step 2** initializes the iteration (or generation) counter, followed by the population initialization in **Step 3**. The population is randomly initiated, taking into account the constraints (23)-(25). **Step 4** initializes the individual counter, and for each individual ind_i, a fitness function fit_i is calculated, as explained in **5** to **7**.

The first procedure to calculate the fitness function is, in **Step 5**, to execute the algorithm for the probabilistic analysis of the stability of the small signal discussed in Sect. 2.4 and Fig. 4. In this step, the uncertainties of wind and load generation are included in the analysis. Once the probabilistic analysis is complete, the probabilities of security ($P_r\left\{\xi_{\min} \geq \xi_d\right\}$) and stability ($P_r\left\{\sigma_{\max} < 0\right\}$) are calculated in **Step 6**. The fitness function is calculated in **Step 7** as discussed in Sect. 3.2.

In **Step 8**, it is checked if all individuals were evaluated. If not, the individual counter is increased in **Step 9** and **Steps 5** to **7** are carried out until all individuals have been evaluated.

Once all individuals are evaluated for a given generation/iteration t, the tuning process is finished in **Step 13**. On the other hand, the algorithm follows to **Step 11** to update the iteration counter and **Step 12** to update the population of individuals according to the PSO method discussed in [41].

4 Case study

4.1 System description

The New-England test system, depicted in Fig. 7, will be used to discuss the results derived from the proposed approach. Comprising 39 nodes and ten generators, the detailed data for this system can be accessed in [33, 36, 43]. In the base case, this system has a total load of 6097.1 MW and 1408.9 MVAr, with active power generation of 6140.8 MW. In this specific case study, a wind generator with a dispatch capacity

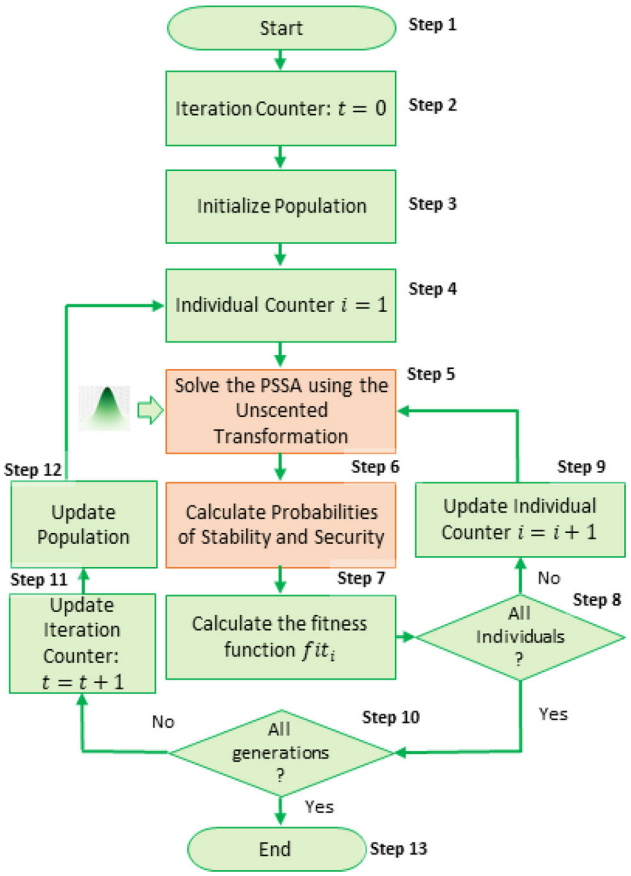

Fig. 6 Flowchart—optimization appraoch

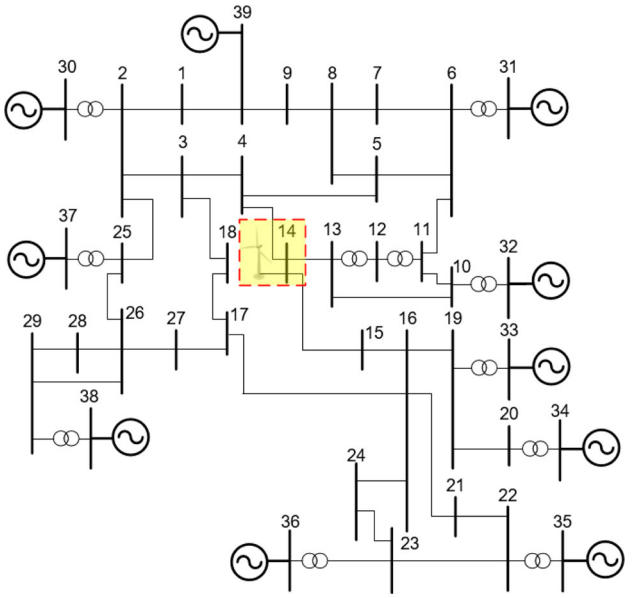

Fig. 7 New-England test system

Table 2 Open-loop electromechanical eigenvalues for the base case scenario

Eigenvalue λ_i	ξ_i (%)
$-0.1699 \pm j8.4996$	2.00
$-0.2414 \pm j8.5012$	2.84
$-0.2162 \pm j8.3441$	2.59
$0.0646 \pm j7.0392$	−0.92
$-0.1339 \pm j7.0707$	1.89
$-0.0313 \pm j6.6870$	0.47
$0.1787 \pm j6.2090$	−2.88
$0.1197 \pm j5.9955$	−2.00
$0.2045 \pm j3.3790$	**-6.04**

of 920 MW is placed at node 14, representing approximately 15% of the active power generation of the base case [44]. The unity power factor is adopted for the wind generator.

For the power system stabilizer (PSS) tuning process, both loads and wind generation are assumed to follow a normal distribution. The same assumptions have been made in [15, 22, 23, 38]. The mean values are set equal to the base case values, and the standard deviations are established at 5% of these mean values. In particular, the generator located at node 39 represents an equivalent system and is therefore excluded from receiving a PSS.

4.2 Parameters of the optimization methods

In the specialized literature, it is known that parameterization of a metaheuristic is essential for securing high-quality solutions. Given that this parameterization is specific to a problem being addressed, the process is inherently empirical, often necessitating significant time investment from the user. In this study, the authors relied on the standard parameters delineated in the literature for PSO. To determine the optimal population size and the number of generations, we set a benchmark of 500 executions of the fitness function. Based on this, the following parameters were established:

- *PSO*: 25 particles, 20 iterations ($25 \times 20 = 500$), $c_1 = c_2 = 2$ (acceleration constants), $\omega_{\max} = 0.9$, $\omega_{\min} = 0.4$ (inertia constants).

4.3 Open-loop eigenvalues in the base case

Deterministic small-signal analysis (see Sect. 2.1), considering the base case condition, reveals an unstable operation with a damping ratio of −6.0421% ($\xi_{min} = -6.0421\%$) and a spectral abscissa of +0.2045 ($\sigma_{max} = 0.2045$). Table 2 gives all electromechanical eigenvalues for the base condition that are plotted in Fig. 8.

The necessary action involves either a deterministic or probabilistic design of the power system stabilizers. The deterministic tuning is extensively discussed in the literature [34, 35]. Studies [9, 21, 45] indicate that the deterministic

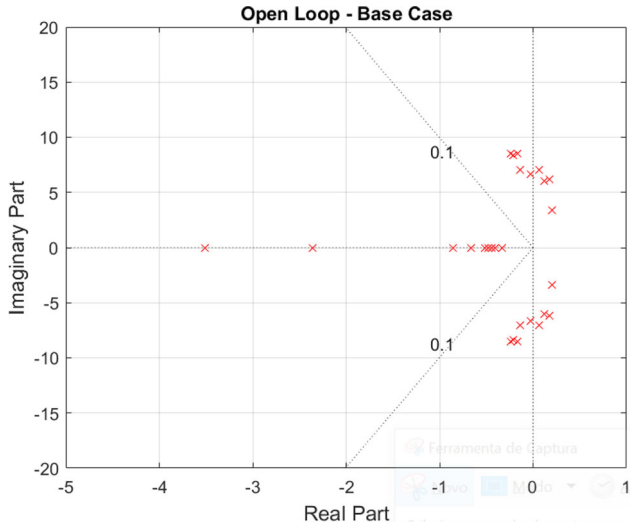

Fig. 8 Open-Loop eigenvalues for the base case scenario

Table 4 Deterministic validation of the probabilistic design *

Caso	Dominant eigenvalue	ξ_{min} (%)
01	$-0.74843 \pm j7.1266$	10.445
02	$-0.75359 \pm j7.1335$	10.506
03	$-0.77348 \pm j7.1018$	10.827

•[*] Values in this table are obtained using the deterministic approach in Sect. 2.1 using the PSS parameters of Table 15

Table 5 Deterministic validation of the deterministic design *

Caso	Dominant eigenvalue	ξ_{min} (%)
01	$-0.88385 \pm j8.4227$	10.436
02	$-0.24738 \pm j3.1418$	7.8497
03	$-0.73759 \pm j7.1454$	10.268

•[*] Values in this table are obtained using the deterministic approach in Sect. 2.1 using the PSS parameters of Table 16

design may not be appropriate in the presence of uncertainties in power loads and renewable generations. In such instances, the probabilistic tuning presented in this paper is particularly compelling, given the low computational burden required by the unscented transformation.

In this paper, the design of power system stabilizers, for the base case, is carried out using two approaches: (*i*) the proposed probabilistic approach and the (*ii*) the deterministic one presented in Appendix B. A target damping ratio of 10% ($\xi_d = 10\%$) is considered.

It is important to emphasize that the deterministic approach aims at positioning the dominant eigenvalue (that with ξ_{min}) in the complex plane so that ξ_{min} is close to ξ_d in the base case. In this case, the deterministic method does not consider the probabilities of security and stability in the design stage.

Table 14, in Appendix C, presents the limits utilized during the design process. Both load and renewable generation are modeled with a mean equal to their nominal values and a standard deviation of 5% of these mean values.

4.4 Deterministic validation of the results

Tables 15 and 16, in Appendix C, displays the optimized parameters obtained using the probabilistic and the deterministic approaches, respectively. It is important to note that these designs must be validated considering other operating conditions to assess the robustness of the controller, as discussed in [35]. Table 3 presents the operating conditions used for tuning (the base case) and the other conditions used for the assessment stage.

Table 4 presents the dominant eigenvalue and the minimum damping ratio for each operating condition in Table 3. These values are obtained from a simple deterministic evaluation of the small-signal stability (when uncertainties are not considered in the analysis as discussed in Sect. 2.1). However, the PSS's parameters are provided by the proposed probabilistic design. It is essential to notice that in both scenarios 01 (base case used in the tuning stage) and 02 and 03 (used for assessment), the system is stable and secure (with $\xi_{min} > \xi_d$). It shows the robustness of the proposed approach in ensuring security in scenarios not considered in the tuning stage.

However, the deterministic design, whose results are presented in Table 5, could not provide a secure condition (with $\xi_{min} < \xi_d$) in Scenario 02 (associated with the reduction of load and wind generation).

To ensure completeness, the eigenvalues of the closed-loop operation are presented for each scenario in Table 3, as shown in Figs. 9 through 11. In these figures, the red crosses indicate the closed-loop eigenvalues considering the PSS tuned by the deterministic design, while the blue crosses are associated with the probabilistic tuning. A line in the

Table 3 Operating conditions considered

Caso	Operating condition	Information
01	Base case	Used in the tuning stage
02	Load reduction (20%) and wind generation reduction (100%)	Used to assess the PSS's robustness
03	Load increase (50%) and wind generation constant (920MW)	Used to assess the PSS's robustness

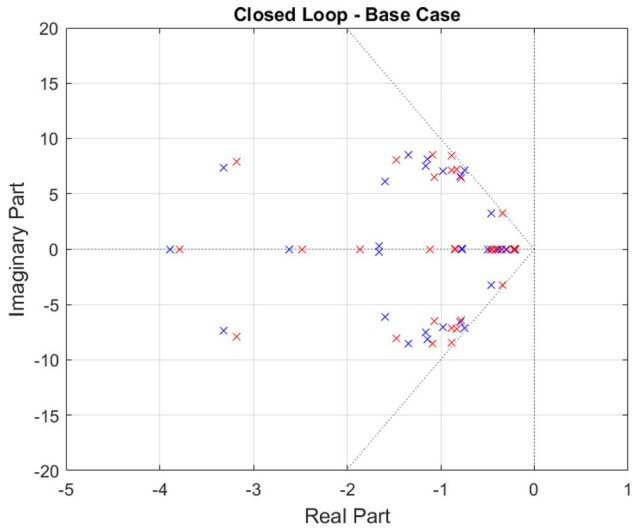

Fig. 9 Closed-loop eigenvalues for the base case scenario: probabilistic (blue) and deterministic (red) (color figure online)

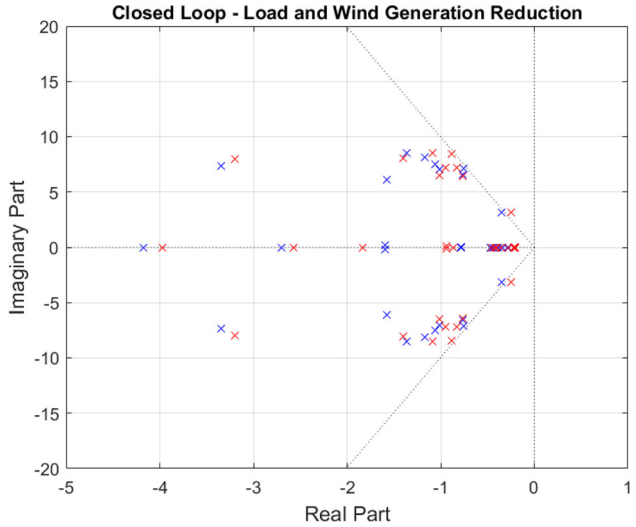

Fig. 10 Closed-loop eigenvalues for the second scenario: probabilistic (blue) and deterministic (red) (color figure online)

complex plane indicates eigenvalues with a damping ratio exceeding 10%. Both probabilistic and deterministic controllers were analyzed for each scenario. Figure 10 correlates with the results in Table 5, revealing a complex eigenvalue with a damping ratio below the safe threshold of 10% (specifically, 7.8497%) when employing deterministic controllers.

4.5 Probabilistic validation of the results

The obtained results using the deterministic and the probabilistic approaches were previously validated from the deterministic point of view. This validation shows that the probabilistic approach was able to provide a secure operation for scenarios that have not been considered in the design

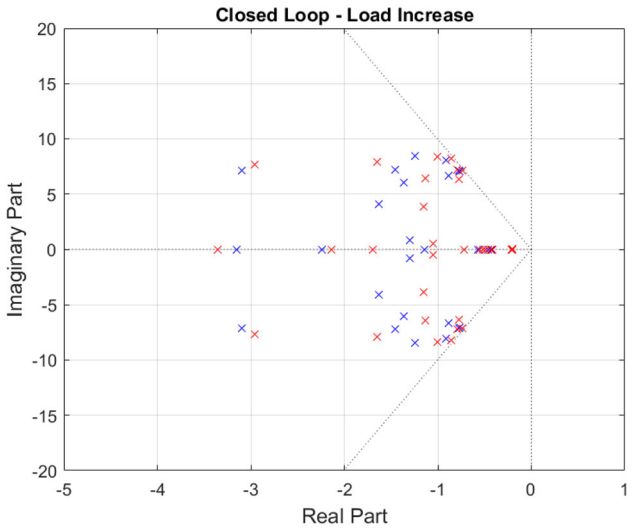

Fig. 11 Closed-loop eigenvalues for the third scenario: probabilistic (blue) and deterministic (red) (color figure online)

stage. To assess the controller's robustness in an uncertain environment, the probabilistic small-signal analysis will be carried out using the unscented transformation (flowchart in Fig. 4 in Sect. 2.4). For this purpose, the following strategy is presented:

1 the three scenarios from Table 3 are considered;
2 the mean values of loads and wind generations are set equal to the updated powers in the item (1);
3 the standard deviations are established at 2.5%, 5% and 10% of these mean values;
4 it should be emphasized that only case 01 (base case) was considered in the design stage. In addition, for the probabilistic design, only one uncertainty level (standard deviation of 5%) was employed in the design stage.

The following points summarize the observations in the probabilistic validation:

- the controller's parameters designed by both design approaches (probabilistic and deterministic) allowed a stable operation no matter the operation condition and uncertainty level of input variables (loads and wind generation). It can be seen in Tables 6, 7, and 8 that the probability of stability ($P_r\{\sigma_{\max} < 0\}$) achieved the maximum value (100%);
- regarding the probability of security ($P_r\{\xi_{\min} \geq \xi_d\}$), as one can see in Table 9, the proposed approach (probabilistic design), provided probabilities of 100% in the base case (scenario 01) for uncertainties levels of 2.5% and 5%. It is important to note that the likelihood of achieving the desired minimum damping ratio of 10% diminishes to 84.9013% when the uncertainty level is

Table 6 Impact of uncertainty on spectral abscissa (Scenario 01: base case)

	Probabilistic design			Deterministic design		
	$\mu_{\sigma_{\max}}$	$\sigma_{\sigma_{\max}}$	$P_r\{\sigma_{\max} < 0\}$	$\mu_{\sigma_{\max}}$	$\sigma_{\sigma_{\max}}$	$P_r\{\sigma_{\max} < 0\}$
2.5%	−0.2035	1.8883e−05	100%	−0.2023	9.0868e−06	100%
5.0%	−0.2035	3.8046e−05	100%	−0.2023	1.8199e−05	100%
10.0%	−0.2035	7.8491e−05	100%	−0.2014	6.0701e−03	100%

Table 7 Impact of uncertainty on spectral abscissa (Scenario 02: load and wind generation reduction)

	Probabilistic design			Deterministic design		
	$\mu_{\sigma_{\max}}$	$\sigma_{\sigma_{\max}}$	$P_r\{\sigma_{\max} < 0\}$	$\mu_{\sigma_{\max}}$	$\sigma_{\sigma_{\max}}$	$P_r\{\sigma_{\max} < 0\}$
2.5%	−0.2036	1.2388e−05	100%	−0.2023	6.7419e−06	100%
5.0%	−0.2036	2.4793e−05	100%	−0.2020	0.0031	100%
10.0%	−0.2030	0.0047	100%	−0.1999	0.0119	100%

Table 8 Impact of uncertainty on spectral abscissa (Scenario 03: load increase)

	Probabilistic design			Deterministic design		
	$\mu_{\sigma_{\max}}$	$\sigma_{\sigma_{\max}}$	$P_r\{\sigma_{\max} < 0\}$	$\mu_{\sigma_{\max}}$	$\sigma_{\sigma_{\max}}$	$P_r\{\sigma_{\max} < 0\}$
2.5%	−0.2030	4.191e−05	100%	−0.2022	1.1437e−05	100%
5.0%	−0.2030	8.4175e−05	100%	−0.2022	2.3343e−05	100%
10.0%	−0.2030	1.8053e−04	100%	−0.2022	5.1059e−05	100%

heightened. Figure 12 provides a comparative view of the (probability density functions) PDFs at varying levels of uncertainty when the parameters provided by the probabilistic approach are considered. However, for the deterministic design, the security probabilities are lower than those obtained in the probabilistic design, emphasizing the importance of the proposed approach in this paper;

- from Table 10, it is possible to see that under load and wind power generation reduction, the probability of security is nearly zero when the parameters provided by the deterministic approach are employed. Although the probability $P_r\{\xi_{\min} \geq \xi_d\}$ is also reduced when the parameters from the proposed probabilistic approach are used, a safe level is obtained. Finally, as given in Table 11, under load increase, the PSSs adjusted by using a probabilistic approach also provide greater levels of security.

4.6 Validation considering the Monte Carlo Simulation

As detailed in Sect. 2.4, the total number of uncertain variables is $n = 2nb + nren = 2 \times 39 + 1 = 79$. In this context, the unscented transformation utilizes a set of $2n + 1 = 159$ sigma points, which are deterministically calculated samples. Consequently, 159 deterministic modal analyses are performed for each probabilistic small-signal analysis. This

Table 9 Impact of uncertainty on damping ratio (Scenario 01: base case)

	Probabilistic design			Deterministic design		
	$\mu_{\xi_{\min}}$	$\sigma_{\xi_{\min}}$	$P_r\{\xi_{\min} \geq \xi_d\}$	$\mu_{\xi_{\min}}$	$\sigma_{\xi_{\min}}$	$P_r\{\xi_{\min} \geq \xi_d\}$
2.5%	10.445%	0.011%	100.00%	10.333%	0.214%	94.04%
5.0%	10.447%	0.023%	100.00%	10.227%	0.438%	69.81%
10.0%	10.393%	0.381%	84.90%	10.00%	0.931%	50.10%

Table 10 Impact of uncertainty on damping ratio (Scenario 02: load and wind generation reduction)

	Probabilistic design			Deterministic design		
	$\mu_{\xi_{\min}}$	$\sigma_{\xi_{\min}}$	$P_r\{\xi_{\min} \geq \xi_d\}$	$\mu_{\xi_{\min}}$	$\sigma_{\xi_{\min}}$	$P_r\{\xi_{\min} \geq \xi_d\}$
2.5%	10.495%	0.092%	100%	7.848%	0.260%	0
5.0%	10.427%	0.277%	93.84%	7.843%	0.521%	0.0018%
10.0%	10.241%	0.720%	63.10%	7.803%	0.993%	1.35%

Table 11 Impact of uncertainty on damping ratio (Scenario 03: load increase)

	Probabilistic design			Deterministic design		
	$\mu_{\xi_{\min}}$	$\sigma_{\xi_{\min}}$	$P_r\{\xi_{\min} \geq \xi_d\}$	$\mu_{\xi_{\min}}$	$\sigma_{\xi_{\min}}$	$P_r\{\xi_{\min} \geq \xi_d\}$
2.5%	10.777%	0.089%	100%	10.259%	0.073%	99.98%
5.0%	10.717%	0.188%	99.99%	10.222%	0.141%	94.29%
10.0%	10.58%	0.442%	90.53%	10.119%	0.359%	62.97%

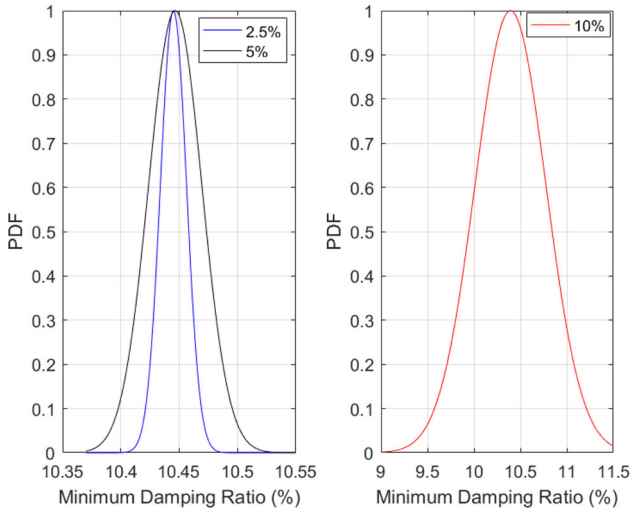

Fig. 12 Comparison of PDF of minimum damping ratio for different levels of uncertainty (scenario 01 using the PSS's parameters provided by the proposed approach)

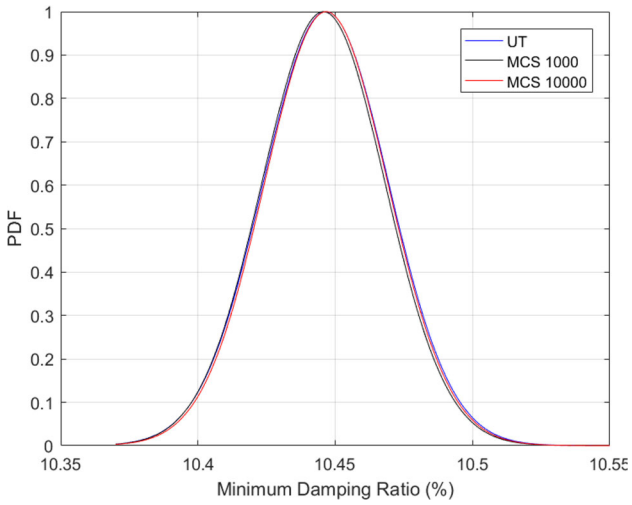

Fig. 13 Comparison of PDF of minimum damping ratio

number is significantly lower than that typically used in Monte Carlo simulation, which ranges from 10^3 to 10^4. This reduction is notable, especially considering the number of individuals and generations in the particle swarm optimization (PSO) process, which involves 25 particles across 20 iterations ($25 \times 20 = 500$). Thus, the total number of deterministic modal analyses in the proposed approach is 159×500.

Considering the base case (scenario 01) and the PSS parameters given in Table 15, the mean and standard deviation of the damping ratio and spectral abscissa obtained from the unscented transformation are compared with those from the Monte Carlo simulation (MCS) in Tables 12 and 13. Despite its substantial computational demand, MCS is a benchmark method. Two distinct MCSs were conducted, one with 10^3 samples and another with 10^4 samples. The findings demonstrate that the proposed methodology, which relies on the unscented transformation using only 159 samples, yields results consistent with those from MCS. The effectiveness of the unscented transformation (UT) is further evidenced in Fig. 13, which displays a close match between the probability density functions of UT and MCS. The same conclusion can be drawn from Table 13 that brings the spectral abscissa.

Table 12 Probabilistic analysis of damping ratio (scenario 01—base case)

	$\mu_{\xi_{\min}}$	$\sigma_{\xi_{\min}}$	$P_r\{\xi_{\min} \geq \xi_d\}$
UT	10.4466	0.0228	100.0000%
MCS (10^3)	10.4457	0.0224	100.0000%
MCS (10^4)	10.4467	0.0224	100.0000%

Table 13 Probabilistic analysis of spectral abscissa (scenario 01—base case)

	$\mu_{\sigma_{\max}}$	$\sigma_{\sigma_{\max}}$	$P_r\{\sigma_{\max} < 0\}$
UT	−0.2035	0.0000	100.0000%
MCS (10^3)	−0.2035	0.0000	100.0000%
MCS (10^4)	−0.2035	0.0000	100.0000%

4.7 Nonlinear time-domain simulation considering the base case

This paper addresses the issue of small-signal stability. However, in agreement with the findings reported in the literature [7], it is also essential to perform a transient stability analysis. Typically, transient stability analysis is executed using nonlinear time-domain simulations. In this section, a simulation of a three-phase fault is performed, considering the base case and optimized controllers (see Tables 15 and

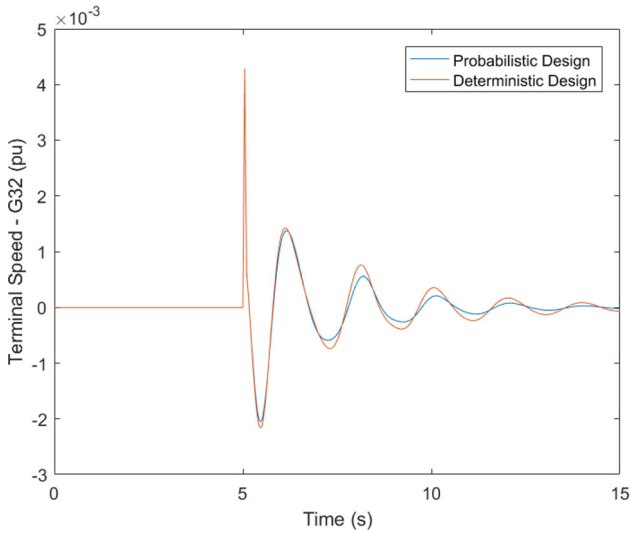

Fig. 14 Terminal speed—generator 32

16). A short circuit is applied on bus 11 for 50 ms, and it is cleared by opening the transmission line 10–11 after the same duration, followed by a reclosure after another 50 ms.

Figure 14 illustrates the behavior of the terminal speed for generator 32, in the base case, since it is close to the faulted line. It is calculated with respect to generator 39 ($\Delta\omega_{32-39}$). It is possible to see that the probabilistic tuning provided a slightly better solution (damped oscillation).

5 Conclusion

The proposed approach for the probabilistic design of conventional power system stabilizers, combining particle swarm optimization and unscented transformation, yielded promising results. First, it was observed that the unscented transformation requires fewer samples to evaluate probabilistic small-signal stability compared to the Monte Carlo simulation. This efficiency highlights the UT's effectiveness. Second, when comparing the results of UT and MCS, including mean values, standard deviation, probabilities of satisfying security (minimum damping ratio) and stability (spectral abscissa) requirements, and probability density functions, a good agreement was found between both methods. This indicates the reliability of UT in probabilistic assessments. In addition, the probabilistic proposed approach provided better robustness than the deterministic approach, mainly for operating conditions not considered in the design stage. Since the probability of meeting the security requirement might be less than 100% for uncertainty levels not considered in the design, future works will be focused on considering a multi-scenario probabilistic approach. Lastly, nonlinear time-domain simulations confirmed the feasibility of the results in terms of angular transient stability, validating the practical applicability of the proposed approach.

Appendix A

This appendix presents the generator model employed in this paper. It is a third-order model comprising Eqs. (31)–(33) (for a given generator k). Equation (34) describes the first-order model of the automatic voltage regulator in Fig. 1 [7].

$$\Delta\dot{\delta}_k = \omega_s \cdot \Delta\omega_k \tag{31}$$

$$\Delta\dot{\omega}_k = \frac{\Delta P_{mk}}{2H_k} - \frac{\Delta P_{gk}}{2H_k} - \frac{D_k}{2H_k} \cdot \Delta\omega_k \tag{32}$$

$$\Delta\dot{E}'_{qk} = -\frac{\Delta E'_{qk}}{T'_{d0k}} - \frac{\left(X_{dk} - X'_{dk}\right)}{T'_{d0k}} \cdot \Delta I_{dk} + \frac{\Delta E_{FDk}}{T'_{d0k}} \tag{33}$$

$$\Delta\dot{E}_{FDk} = -\frac{\Delta E_{FDk}}{T_{Ak}} + \frac{K_{Ak}}{T_{Ak}} \cdot (\Delta V_{REFk} - \Delta V_k + \Delta V_{PSSk}) \tag{34}$$

where

- D_k is the damping constant (pu);
- ΔE_{FDk} is the field voltage (exciter output) (pu);
- $\Delta E'_{qk}$ is the internal voltage (pu);
- H_k is the inertia constant (s);
- ΔI_{dk} is the d-axis stator current (pu);
- ΔP_{mk} is the mechanical power (pu);
- ΔP_{gk} is the electrical power (pu);
- T'_{d0k} is the d-axis open-circuit time constant (s);
- X'_{dk} is the d-axis transient reactance (pu);
- X_{qk} is the q-axis synchronous reactance (pu);
- ΔV_{REFk} is the reference voltage (pu);
- ΔV_k is the terminal voltage (pu);
- ΔV_{PSSk} is the PSS voltage (pu);
- ω_s is the synchronous speed (rad/s);
- $\Delta\omega_k$ is the rotor speed deviation (pu).

Appendix B

The deterministic approach for the design of power system stabilizers is presented in (35)-(40). It aims to allocate the dominant eigenvalue (associated with the minimum damping ratio) in a region where $\xi_{\min}$ is close to ξ_d, ensuring a level of security and stability, as given in (36)-(37).

$$\min f(x) = \quad |\, \xi_{\min} - \xi_d \,| \tag{35}$$

$$\xi_{\min} \geq \xi_d \tag{36}$$

$$\sigma_{\max} < 0 \tag{37}$$

$$K_p^{\min} \leq K_p \leq K_p^{\max} \tag{38}$$

$$\alpha_p^{\min} \leq \alpha_p \leq \alpha_p^{\max} \tag{39}$$

$$\omega_p^{\min} \leq \omega_p \leq \omega_p^{\max} \tag{40}$$

The solution of (35)-(40) is carried out using PSO, where (38)-(40) are treated by the optimization method. Each individual is evaluated by employing the deterministic analysis of small-signal stability discussed in Sect. 2.1, where Eqs. (36)–(37) are integrated as penalties within the objective function of (35) in case of violations.

Appendix C

This appendix presents the limits of the optimization variables in Table 14. The parameters adjusted by the probabilistic and deterministic approaches are presented in Tables 15 and 16.

Table 14 Limits of PSS parameters

	K_p	α_p	ω_p
Lower	0.01	0.10	1.25
Upper	40	10	30

Table 15 PSS parameters—probabilistic design

	K_p	α_p	ω_p
30	40.0000	10.0000	7.5926
31	16.8832	10.0000	13.5350
32	30.4979	7.8315	10.6940
33	36.9414	10.0000	19.1145
34	24.8381	9.9401	23.8874
35	33.1318	9.0207	20.7493
36	22.4296	5.0425	16.0664
37	11.9922	9.0746	7.9857
38	21.6856	3.9891	30.0000

Table 16 PSS parameters—deterministic design

	K_p	α_p	ω_p
30	31.4354	10.0000	3.4672
31	28.7777	6.8904	14.5810
32	40.0000	8.9793	14.1224
33	13.1306	10.0000	11.1220
34	16.2801	4.4570	24.2646
35	30.5641	5.2943	13.3238
36	22.8738	5.9281	19.6086
37	18.6969	6.1518	12.3841
38	18.6135	3.6758	30.0000

Appendix D

To elucidate the probabilistic small-signal stability analysis process, detailed in Sect. 2.3 (Fig. 3), Fig. 15 is presented. This analysis considers a scenario in which two generators are equipped with a single power system stabilizer (PSS), as outlined in **Step 1**. The primary goal is to compute the mean and standard deviations of σ_{max} and ξ_{min}. Accordingly, a sample is generated in **Step 2**, followed by the calculations for σ_{max} and ξ_{min} in **Steps 3** to **6**. Given the Monte Carlo simulation (MCS) framework, **Steps 3** to **6** are repeated across multiple samples. The process culminates in the computation of the mean and standard deviations.

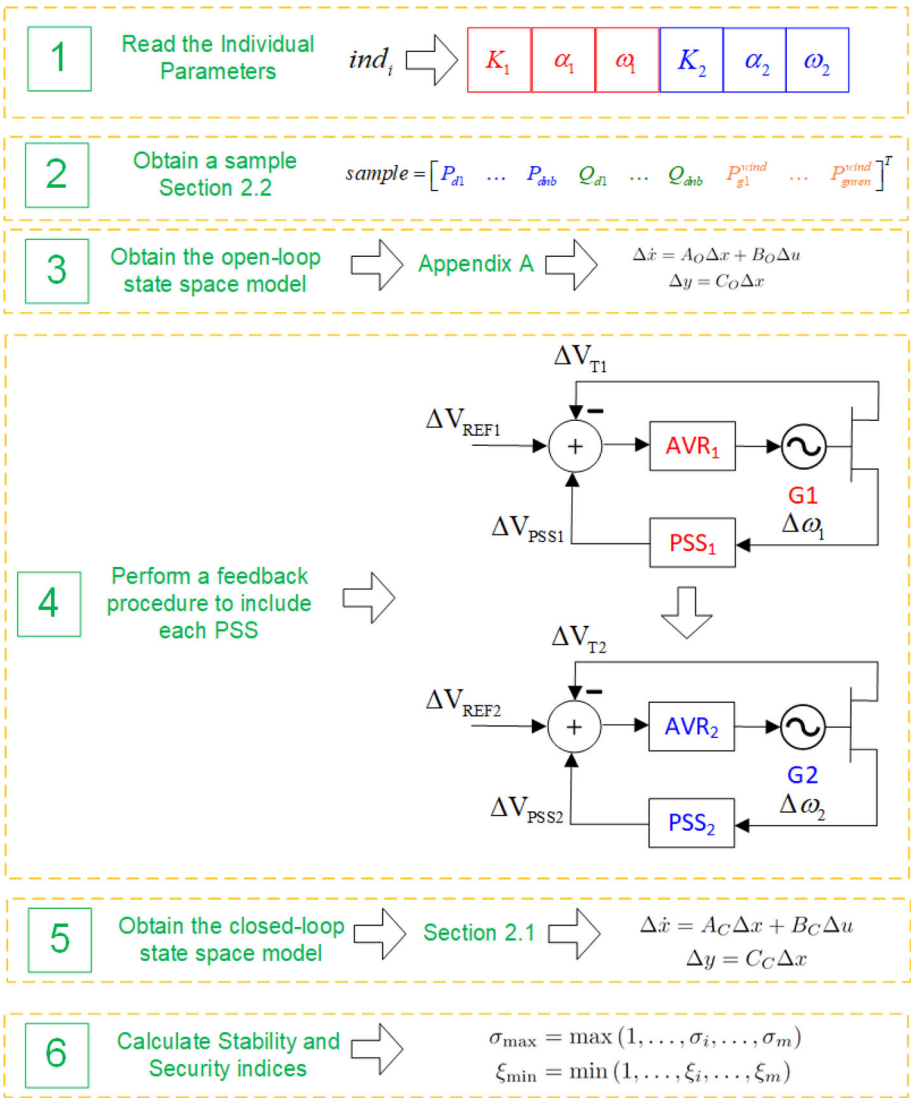

Fig. 15 Calculation of σ_{max} and ξ_{min} in MCS environment

Acknowledgements The support from INERGE, FAPEMIG (APQ-02245-18), CAPES and CNPq is greatly acknowledged.

References

1. Rogers G (2000) Power System Oscillations. Springer, Boston, MA https://doi.org/10.1007/978-1-4615-4561-3
2. Demello F, Concordia C (1969) Concepts of synchronous machine stability as affected by excitation control. IEEE Trans Power Appar Syst 88(4):316–329. https://doi.org/10.1109/TPAS.1969.292452
3. Kundur P, Klein M, Rogers GJ, Zywno MS (1989) Application of power system stabilizers for enhancement of overall system stability. IEEE Trans Power Syst. https://doi.org/10.1109/59.193836
4. Ibrahim NMA, El-said EA, Attia HEM, Hemade BA (2023) Enhancing power system stability: an innovative approach using coordination of FOPID controller for PSS and SVC FACTS device with MFO algorithm. Electr Eng. https://doi.org/10.1007/s00202-023-02051-7
5. He P, Pan Z, Fan J, Tao Y, Wang M (2023) Coordinated design of PSS and multiple FACTS devices based on the PSO-GA algorithm to improve the stability of wind-PV-thermal-bundled power system. Electr Eng. https://doi.org/10.1007/s00202-023-02055-3
6. Kundur P (1994) Power System Stability and Control, 1st edn. McGraw-Hill, Nova Iorque, Nova York
7. Sauer PW, Pai MA, Chow JH (2017) Power System Dynamics and Stability: With Synchrophasor Measurement and Power System Toolbox 2e. Wiley, Champaign, Illinois https://doi.org/10.1002/9781119355755. https://onlinelibrary.wiley.com/doi/book/10.1002/9781119355755
8. Singh V, Moger T, Jena D (2022) Uncertainty handling techniques in power systems: a critical review. Electr Power Syst Res. https://doi.org/10.1016/j.epsr.2021.107633
9. Bian XY, Geng Y, Lo KL, Fu Y, Zhou QB (2016) Coordination of PSSs and SVC damping controller to improve probabilistic small-signal stability of power system with wind farm integration. IEEE Trans Power Syst 31(3):2371–2382. https://doi.org/10.1109/TPWRS.2015.2458980
10. Rafique Z, Khalid HM, Muyeen SM, Kamwa I (2022) Bibliographic review on power system oscillations damping: an era of conventional grids and renewable energy integration. Int J Electr Power Energy Syst. https://doi.org/10.1016/j.ijepes.2021.107556

11. Roald LA, Pozo D, Papavasiliou A, Molzahn DK, Kazempour J, Conejo A (2023) Power systems optimization under uncertainty: a review of methods and applications. Electr Power Syst Res. https://doi.org/10.1016/j.epsr.2022.108725
12. Huang H, Chung CY, Chan KW, Chen H (2013) Quasi-monte carlo based probabilistic small signal stability analysis for power systems with plug-in electric vehicle and wind power integration. IEEE Trans Power Syst. https://doi.org/10.1109/TPWRS.2013.2254505
13. Ahmadi H, Seifi H (2014) Probabilistic tuning of power system stabilizers considering the wind farm generation uncertainty. Int J Electr Power Energy Syst. https://doi.org/10.1016/j.ijepes.2014.06.036
14. Ke D, Chung CY (2016) Design of probabilistically-robust wide-area power system stabilizers to suppress inter-area oscillations of wind integrated power systems. IEEE Trans Power Syst 31(6):4297–4309. https://doi.org/10.1109/TPWRS.2016.2514520
15. Chabane Y, Ladjici AA, Hellal A, Dookhitram K (2020) Cooperative coevolutionary algorithms for optimal PSS tuning based on Monte-Carlo probabilistic small-signal stability assessment. Int Trans Electr Energy Syst. https://doi.org/10.1002/2050-7038.12618
16. Shim JW, Verbic G, Hur K (2020) Stochastic eigen-analysis of electric power system with high renewable penetration: impact of changing inertia on oscillatory modes. IEEE Trans Power Syst. https://doi.org/10.1109/TPWRS.2020.3000577
17. Amaral TS, Gomes S, Borges CLT (2021) Reliability evaluation of bulk power systems with wind generation using small signal stability analysis. Int J Electr Power Energy Syst. https://doi.org/10.1016/j.ijepes.2021.106840
18. Fatah Mochamad R, Preece R, Hasan KN (2022) Probabilistic multi-stability operational boundaries in power systems with high penetration of power electronics. Int J Electr Power Energy Syst. https://doi.org/10.1016/j.ijepes.2021.107382
19. Santos M, Calvaittis Santana G, DeCampos M, Sperandio M, Sausen PS (2021) Performance of controller designs in small-disturbance angle stability of power systems with parametric uncertainties. IEEE Lat Am Trans. https://doi.org/10.1109/TLA.2021.9480147
20. Wang Z, Chung CY, Wong KP, Tse CT (2008) Robust power system stabiliser design under multi-operating conditions using differential evolution. IET Gener Trans Distrib 2(5):690. https://doi.org/10.1049/iet-gtd:20070449
21. Gurung S, Jurado F, Naetiladdanon S, Sangswang A (2019) Optimized tuning of power oscillation damping controllers using probabilistic approach to enhance small-signal stability considering stochastic time delay. Electr Eng 101(3):969–982. https://doi.org/10.1007/s00202-019-00833-6
22. Gurung S, Jurado F, Naetiladdanon S, Sangswang A (2020) Comparative analysis of probabilistic and deterministic approach to tune the power system stabilizers using the directional bat algorithm to improve system small-signal stability. Electr Power Syst Res. https://doi.org/10.1016/j.epsr.2019.106176
23. Gurung S, Naetiladdanon S, Sangswang A (2019) Coordination of power-system stabilizers and battery energy-storage system controllers to improve probabilistic small-signal stability considering integration of renewable-energy resources. Appl Sci (Switzerland). https://doi.org/10.3390/app9061109
24. Gurung S, Naetiladdanon S, Sangswang A (2021) A surrogate based computationally efficient method to coordinate damping controllers for enhancement of probabilistic small-signal stability. IEEE Access. https://doi.org/10.1109/ACCESS.2021.3060502
25. Cao R, Xing J, Li Z, Ma H (2024) Probabilistic small signal stability analysis with wind power based on maximum entropy theory. Electr Power Compon Syst. https://doi.org/10.1080/15325008.2024.2310775
26. Julier SJ, Uhlmann JK (2004) Unscented filtering and nonlinear estimation. In: Proceedings of the IEEE, vol. 92, pp. 401–422 . https://doi.org/10.1109/JPROC.2003.823141
27. Hong HP (1998) An efficient point estimate method for probabilistic analysis. Reliab Eng Syst Saf 59:261–267
28. Yi H, Hou Y, Cheng S, Zhou H, Chen G (2007) Power System Probabilistic Small Signal Stability Analysis Using Two Point Estimation Method. In: UPEC 2007, pp. 402–407
29. Soleimanpour N, Mohammadi M (2012) Probabilistic small signal stability analysis considering wind energy. In: Iranian Conference on Smart Grids, pp. 1–6
30. Morshed MJ, Fekih A (2019) A probabilistic robust coordinated approach to stabilize power oscillations in DFIG-based power systems. IEEE Trans Industr Inf. https://doi.org/10.1109/TII.2019.2901935
31. Li L, Jiang H, Yang P, Fan P, Qi P, Kang L (2022) Small signal stability analysis and optimize control of large-scale wind power collection system. IEEE Access. https://doi.org/10.1109/ACCESS.2022.3158335
32. Vijaya VL, Manyala RR, Mangipudi SK (2020) Design of a robust PID-PSS for an uncertain power system with simplified stability conditions. Prot Control Mod Power Syst. https://doi.org/10.1186/s41601-020-00165-9
33. Pai MA (1989) Energy Function Analysis for Power System Stability. Springer, Boston, MA . https://doi.org/10.1007/978-1-4613-1635-0
34. Peres W, De Oliveira EJ, Passos Filho JA, Da Silva Junior IC (2015) Coordinated tuning of power system stabilizers using bio-inspired algorithms. Int J Electr Power Energy Syst 64:419–428. https://doi.org/10.1016/j.ijepes.2014.07.040
35. Peres W, Silva Júnior IC, Passos Filho JA (2018) Gradient based hybrid metaheuristics for robust tuning of power system stabilizers. Int J Electr Power Energy Syst 95:47–72. https://doi.org/10.1016/j.ijepes.2017.08.014
36. Peres W, da Costa NN (2020) Comparing strategies to damp electromechanical oscillations through STATCOM with multi-band controller. ISA Trans 107:256–269. https://doi.org/10.1016/j.isatra.2020.08.005
37. Parreiras Masseran Antunes TJ, Gomes Junior S, Nery Taranto G (2017) Damping nomogram method for small-signal security assessment of power systems. IEEE Lat Am Trans 15(5):877–883. https://doi.org/10.1109/TLA.2017.7910201
38. Aien M, Fotuhi-Firuzabad M, Aminifar F (2012) Probabilistic load flow in correlated uncertain environment using unscented transformation. IEEE Trans Power Syst 27(4):2233–2241. https://doi.org/10.1109/TPWRS.2012.2191804
39. Valverde G, Terzija V (2011) Unscented Kalman filter for power system dynamic state estimation. IET Gener Transm Distrib 5(1):29–37. https://doi.org/10.1049/iet-gtd.2010.0210
40. Peres W (2024) A probabilistic load flow for unbalanced three-phase islanded microgrids using unscented transformation. Int J Electr Power Energy Syst 155:109554. https://doi.org/10.1016/j.ijepes.2023.109554
41. Eberhart R, Kennedy J (1995) New optimizer using particle swarm theory. In: Proceedings of the International Symposium on Micro Machine and Human Science https://doi.org/10.1109/mhs.1995.494215
42. Montgomery DC, Runger GC (1994) Applied statistics and probability for engineers. Eur J Eng Educ. https://doi.org/10.1080/03043799408928333
43. Peres W, Passos Filho JA, Coelho FCR, Poubel RPB, Costa JNN (2021) Dynamic transmission capability calculation using bioinspired optimization. Int J Electr Power Energy Syst. https://doi.org/10.1016/j.ijepes.2021.107227
44. Tavela FM, Filho JAP, Avila OF (2022) Assessment of the impact of wind generation intermittency on electric power systems through

security regions. J Control Autom Electr Syst 33(3):982–997. https://doi.org/10.1007/s40313-021-00870-2
45. He P, Arefifar SA, Li C, Tao Y (2019) Small signal stability analysis of doubly-fed induction generator-integrated power systems based on probabilistic eigenvalue sensitivity indices. IET Gener Transm Distrib. https://doi.org/10.1049/iet-gtd.2018.5265